AUTHOR'S POST PRINT (Romeo Colour: Green)
Num. Heat Transfer Part B - Fundamentals (ISSN: 1040-7790), 43 (4): 373-401 (2003).
DOI: 10.1080/713836224
Publisher version available at
http://www.tandfonline.com/doi/abs/10.1080/713836224

Complex dynamics of rhythmic patterns and sedimentation of organic crystals: a new numerical approach

M. Lappa[*] and D. Castagnolo

MARS (Microgravity Advanced Research and Support Center)
Via Gianturco 31 - 80146, Napoli, Italy
[*]current e-mail address: marcello.lappa@strath.ac.uk

Abstract

This paper deals with the mathematical modelling and numerical simulation of the complex phenomena related to the crystallization of an organic macromolecular substance due to solubility modulation (lysozyme). Novel mathematical models and numerical strategies are introduced to simulate the protein nucleation and further precipitation (or resolution) according to the concentration distribution and in particular to take into account the motion of the crystals due to the combined effect of gravitational force and viscous drag if the sedimenting process is allowed (protein reactor free of gel). The numerical simulations show that gellified lysozyme reacts to produce "spaced deposits". The phenomenon is characterized by a certain degree of periodicity in time and in space (Liesegang patterns). If the gel matrix is not present, crystals settle in the growth chamber. In this case, due to solutal buoyancy forces, a very complex convection pattern arises whose dynamics depend upon the nucleation phenomena occurring in the bulk of the protein chamber.

Running head: periodic precipitation and sedimentation

Nomenclature list

C_{lys}	protein concentration
C_{NaCl}	salt concentration
$C_{lys(o)}$	initial value of protein concentration
$C_{NaCl(o)}$	initial value of salt concentration
D_{lys}	lysozyme diffusion coefficient
D_{NaCl}	salt diffusion coefficient
H	height of the geometrical configuration
h	average position of the gel interface along y
g	gravity acceleration
L	length of the chambers
$M_{grain(o)}$	mass of the solid particle at the initial time
M_{grain}	mass of the solid particle
p	pressure
R(t)	radius of the solid particle
Ra	Rayleigh number
S	solubility or “saturation level”
Sc	Schmidt number
t	time
V	velocity field
V_{grain}	velocity of the sedimenting crystal

Greek Symbols

α	growth coefficient
β	resolution coefficient
β_{lys}	lysozyme solutal expansion coefficient
β_{NaCl}	salt solutal expansion coefficient
χ	porosity of the solid phase
δ_g	decrement of protein concentration due to further precipitation
δ_i	increment of protein concentration due to crystal dissolution
ϕ	phase variable
η	supersaturation limit
μ	dynamic viscosity
ν	kinematic viscosity
ρ_c	density of the crystal
ρ_{H_2O}	density of water
ρ_L	density of the liquid solution
ρ_P	protein mass density in the crystal
τ	relative importance of induction time and characteristic diffusion time
ξ	function modelling the interface curvature

Subscripts

lys	lysozyme
NaCl	Salt
Grain	solid phase
(o)	initial value

Superscripts

n	time step
m	operation index

1. INTRODUCTION

Periodic precipitation is a generic term for material deposition processes which occur intermittently in terms of time or space or (generally) both. These processes represent a special case of fashionable topic: oscillatory reactions, with practical implications in crystal growth and material preparation, and a theoretical kinship with the complex of problems that come under the heading “order out of chaos”.

In case precipitation is induced by mutual diffusion of reagents, the related phenomenon is characterized by a certain degree of periodicity in time and/or in space. The term “periodic”, however, should be interpreted with caution and tolerance. Strictly speaking, it demands a period (i.e. a constant time or space interval), something that the phenomena here under discussion fail to show. These phenomena are nevertheless “periodic”. The periods are not constant, but they are not random either. Periodic precipitation is often referred to as “Liesegang patterns”, because it was first studied by Liesegang. Liesegang patterns can manifest themselves in a great variety of media and ways.

In the present paper the crystallization process of a macromolecular substance and the related “rhytmic” phenomena will be presented and analyzed under two different conditions, both occurring however when the process is carried out on Earth.

For laboratory research, typically investigators let reagents diffuse in some (preferably inert) environment. In this environment protein reacts to produce “spaced deposits”, each consisting of crystals. Under normal gravity conditions, convection, that would destroy the Liesegang patterns, is prevented by the use of gel (case (1)). Agarose gel turns out to be a particularly suitable diffusion medium, because of its mechanical flexibility and chemical inertness. Moreover due to its mechanical properties, crystals produced due to nucleation are “locked” on the matrix of gel so that sedimentation does not occur.

If the gel matrix is not present, since crystals are denser than the feeding solution, sedimentation occurs and the crystals settle in the growth chamber (case (2)).

In the present paper the periodic precipitation of a protein substance is considered. In the last years great interest has been directed towards crystals of biological macromolecules and in particular towards the crystallization process of protein substances [1-8]. In fact, single crystals with good diffraction properties are needed to achieve high resolution data on protein structure needed for progress in biotech and drug. Typically these crystals are obtained by precipitation from super-saturated solutions with a number of techniques. Aim of this study is to clarify the dynamics of the initial process of protein crystallization, i.e. the initial stage of crystallization in both cases ((1) and (2)).

In the first case a mathematical model is introduced to handle the protein nucleation and further precipitation or resolution according to the concentration distribution. In the second case, further to the previous mathematical modelling and numerical investigation, a novel numerical technique is developed to investigate the motion of the crystals due to the combined effect of gravitational force and viscous drag and the interaction of this motion with the concentration field. The study is initially carried out under the assumption of protein reactor free of buoyancy convection. Finally the model is further improved taking into account the effect of convection due to solutal buoyancy forces arising from the protein depletion.

The present strategy can be seen as a very hybrid technique and considered an earliest example of a new class of VOF methods specifically developed for the case of organic growth from supersaturated solutions due to solubility modulation and sedimentation (OCSVOF Organic Crystal Sedimentation Volume of Fraction Method) that has not appeared in literature until now.

2. STUDY CONFIGURATION

The configuration under investigation consists of a protein solution and a salt solution placed one above the other and separated by an "interface". The interface is strictly related to the presence of agarose gel in the lower solution. The protein is lysozyme and the precipitant agent is NaCl salt (the system being at pH=4.5). The geometrical configuration is a chamber whose length and height are L and H respectively; the interface is placed at $y \cong h$.

For the first case under investigation (no sedimentation allowed) agarose is added to the protein solution in order to avoid crystal sedimentation and convection. The salt solution is located on the top of the protein solution (Fig.1a). For the second case (sedimentation allowed) the salt solution is filled with agarose gel and it is located on the bottom of the protein solution; crystals produced in this case are allowed to sediment on the gel interface (Fig.1b). At the initial time, both solutions are at constant concentration respectively.

Experimentally, the shape of the gel interface cannot be horizontal due to the occurrence of a meniscus which is caused by surface tension effects. A sin function (i.e. $\xi(x)/h=1.1-0.1\sin(\pi x/L)$) is used to model interface curvature in order to have a minimum protruding in the lower chamber at the mean point along the horizontal length of the chamber ($\xi(x=0)=\xi(x=L)$ and the minimum at $x=L/2$). The gel interface is impermeable to the protein. The data used as input for the numerical simulation are shown in Table 1.

3. MATHEMATICAL MODEL AND NUMERICAL METHOD:

3.1 Growth in gel - Governing field equations:

The model is based on the mass balance equations, without consider cross-coupled coefficients, which are two order of magnitude lower at the considered concentration levels. Therefore, in absence of convection, the diffusion of lysozyme is governed by the equation

$$\frac{\partial C_{lys}}{\partial t} = \nabla^2 C_{lys} \qquad (1)$$

A similar equation governs the diffusion of salt (in this case it is assumed that salt does not precipitate in solid phase).

The non-dimensional form of the equations results from scaling the lengths by the horizontal distance between the walls (L), the time by L^2/D_{lys}, (D_{lys} being the lower diffusion coefficient) and the concentrations of protein and salt by their initial values ($C_{lys(o)}$ and $C_{NaCl(o)}$).

The walls and the gel interface are supposed to be impermeable to the protein.

3.2 Organic growth by solubility modulation:

In the case of organic substances, crystal growers usually obtain deposition of material from solution by allowing a "reagent" to diffuse which does not actually react but acts modifying (reducing) the solubility (solubility modulation).

Whenever protein in solute phase and solid crystal co-exist in equilibrium (saturation condition):

$$C_{lys}=S \qquad (3)$$

where S is the solubility and it depends on [NaCl] concentration.

In a saturated solution, two states exist in equilibrium, the solid phase, and one consisting of molecules free in solution. At saturation, no net increase in the proportion of solid phase can accrue since it would be counterbalanced by an equivalent dissolution. Thus ‘crystals do not grow from a saturated solution’. The system must be in a non-equilibrium, or supersaturated state to provide the thermodynamic driving force for crystallization (McPherson [1]).

Solution must by some means be transformed or brought into the supersaturation state whereby its return to equilibrium, forces exclusion of solute molecules into the solid state, the

crystal. As long as C_{lys} <S, more solid material will dissolve if any. If, on the other hand, C_{lys} >S, material will condense on any material already existing and augment its size. The 'growth regime' may be very complex and non-linear.

The nucleation of new material is something else and the features of this phenomenon have to be modeled separately; the term 'precipitation' refers in fact to the composite phenomenon of nucleation and subsequent growth. Growth can take place at concentrations lower that those needed for nucleation, as long as C_{lys}>S. The solution is said to be *supersaturated* when the solute content is greater than S, and the degree of supersaturation σ is defined by $\sigma = C_{lys}/S$.

When there is no pre-existing deposit ([M]), it is generally found that the concentration of protein has to be greater than S to create one spontaneously, say

$$\sigma \geq \eta \qquad (4)$$

where η is called the "*supersaturation limit*" (it is obvious that $\eta > 1$); once nuclei are created, precipitation can continue if $1<\sigma\leq\eta$ and viceversa material can come back to the solute condition if $0<\sigma<1$. In this work it is assumed $\eta=3$. The dependence of S of lysozyme on C_{NaCl} has been determined experimentally (Otàlora and Garcìa Ruiz [6]).

3.3 Discussion:

In the specific case of mass crystallization from a supersaturated solution one must generally accomplish at least two things simultaneously: (a) determine the concentration fields of organic substance and precipitant in the liquid phase and (b) determine the position of the interface between the solid and liquid phases. According to the technique used to address (a) and (b), in principle the numerical procedures able to solve these problems can be divided into different groups.

If the size of the crystals is negligible with respect to the size of the reactor i.e. if the seeds are small and undergo only small dimensional changes with respect to the overall dimensions of the cell containing the feeding solution, the only information associated to each grain is its position and mass. These data can be stored in special arrays (three arrays are needed in this case: the first for the position along x, the second for the position along y and the third for the mass associated to each crystal). However a more elegant approach consists in introducing a non-dimensional phase-field variable ϕ.

This approach accounts for the solid mass stored in the generic computational cell by assigning an appropriate value of ϕ to each mesh point (ϕ=1 computational cell filled with solid mass, ϕ=0 liquid and $0<\phi<1$ for a computational cell containing both liquid and solid phases). The key element for the method is its technique for adjourning ϕ. Upon changing phase, the ϕ-value of the cell containing the crystal is adjusted to account for mass release or absorption, this adjustment being reflected in the protein concentration distribution as either a source or sink. The modelling of these phenomena leads to the introduction of a group of equations. These equations are of algebraic type (Henisch [7]) if the detailed description of the crystal surface morphology is not essential for the problem under investigation (present case) otherwise they are differential equations associated to the attachment kinetics condition used to model mass transfer at the crystal surface (Pusey et al. [4]).

The non-dimensional volume of the crystal mass M stored in a grid cell can be computed as (ρ_P is the protein mass density in the crystal):

$$dv\big|_{stored} = \frac{1}{L^3}\frac{M}{\rho_P} \rightarrow \phi = \frac{dv\big|_{stored}}{dv} \tag{5}$$

where dv is the volume of the computational cell.

3.4 Nucleation and further precipitation

3.4.1. nucleation

According to the crystallization criteria introduced by Henisch and Garcìa Ruiz [5] (algebraic model), once the solid particles [M] are formed it is assumed that they are in equilibrium with protein and salt in liquid phase. Thus the concentration of protein has to satisfy eq. (3), i.e. the solute content of the solution will have to be decremented from the original C_{lys} value to a value which must satisfy eq. (3).

If $\phi^m = 0$ and $\sigma^m = (C_{lys}/S)^m \geq \eta \rightarrow$

$$(C_{lys})^{m+1} = S^m, \quad M_{grain(o)} = \left(C_{lys} - S\right)^m C_{lys(o)} L^3 dv \quad , \quad \phi^{m+1} = \frac{1}{L^3}\frac{M_{grain(o)}}{\rho_P} = \frac{S^m C_{lys(o)}}{\rho_P}(\sigma - 1)^m \quad (6)$$

these algebraic equations, where m superscript is used to indicate subsequent operations for a fixed time, model the nucleation process in a very simple way. We assume that the newly formed solid phase is constituted by only one crystal with mass $M_{grain(o)}$. Of course this assumption is not verified for very large values of supersaturation when an intense precipitation takes place, leading to a large concentration of nuclei. Typically, this occurs when supersaturation is increased very rapidly, with respect to the time needed for nuclei formation (induction time).

The phenomena here under investigation are driven by the diffusion of salt through the gel interface. The nucleation process and further growth, in fact, are strictly associated to the modulation of the supersaturation limit and of the solubility due to salt diffusion. Therefore the characteristic time of the phenomena under investigation is the diffusion time of salt in the protein chamber ($t = h^2/D_{NaCl} \cong 2 \cdot 10^5$ s). The induction time according to Galkin and Vekilov [8] is of the order of $2 \cdot 10^3$ [s]. The relative importance of the two effects (characteristic induction time and characteristic diffusion time) is measured by the non-dimensional parameter:

$$\tau_{r.i} = t_{induction}/t_{NaCl} \cong 10^{-2} \quad (7)$$

Since τ is $O(10^{-2})$, the first effect can be neglected with respect to the latter. This explains why the increase of the supersaturation can be considered slow for the phenomena under investigation and at the same time allows the present mathematical-physical model to assume that if the supersaturation limit is exceeded, the amount of supersaturated protein in liquid phase becomes solid without any time delay (kinetic effects are negligible).

By the technique under investigation a 'suitable' limited degree of supersaturation can be achieved. In very concentrated solutions, in fact, the macromolecules may aggregate as an amorphous precipitate. This result is to be avoided if possible and is indicative that supersaturation has proceeded too extensively or too swiftly.

3.4.2. further growth or resolution

In the presence of a deposit ($\phi>0$), it is highly unlikely that the supersaturation will ever reach η again, but if it is the case, secondary nucleation can occur, with formation of an additional deposit in the computational cell. However it is more likely that, due to salt transport in fluid phase, protein concentration becomes larger than S; in this case the existing deposit would grow; on the other hand, in case protein concentration becomes smaller than S, deposit would begin to re-dissolve. Two adjustable "kinetic" coefficients β ("re-solution coefficient") and α ("growth coefficient") are introduced to handle these phenomena (see Henisch [7]).

If $\phi^m>0$ and $1<\sigma^m<\eta\rightarrow$ further growth:

$(C_{lys})^{m+1} = (C_{lys})^m - \alpha\delta_g$, $\delta_g = (C_{lys} - S)^m$,

$$M_{grain}^{m+1} = M_{grain}^{m} + \alpha\delta_g C_{lys(o)} L^3 dv \;, \qquad \phi^{m+1} = \phi^m + \alpha \frac{S^m C_{lys(o)}}{\rho_P}(\sigma - 1)^m \tag{8a}$$

If $\phi^m>0$ and $\sigma^m<1\rightarrow$ resolution:

$(C_{lys})^{m+1} = (C_{lys})^m + \beta\delta_i$, $\delta_i = (S - C_{lys})^m$,

$$M_{grain}^{m+1} = M_{grain}^{m} - \beta\delta_i C_{lys(o)} L^3 dv \;, \qquad \phi^{m+1} = \phi^m + \beta \frac{S^m C_{lys(o)}}{\rho_P}(\sigma - 1)^m \tag{8b}$$

Kinetic effects may be relevant for large biological molecules, and they may influence growth and dissolution of deposits. To take into account this aspect two cases were considered: a) $\alpha=\beta=1$ (absence of kinetic effects); b) $\beta=(M_{grain(o)}/ M_{grain})^{1/3}$, $\alpha=1-0.9 (M_{grain(o)}/ M_{grain})^{2/3}$.

The β and α expressions in case (b) are introduced in Ref. [7] starting from two "well-known" behaviours: small grains dissolve more easily than large ones, large grains grow more rapidly than small ones. However, no relevant difference was observed from a macroscopic point of view between cases (a) and (b) for the conditions considered in the present simulations. For the present case of complex “periodic” phenomena (rhythmic dynamics) the macroscopic spatio-temporal evolution of the process is mainly driven by the availability of protein in liquid phase (many crystals compete for growth, the related depletion zones intersect and overlap) and by the rhythmic increase and decrease of supersaturation due to the interplay between protein depletion and salt diffusion through the gel interface. For this reason surface kinetics can be neglected while sacrificing little in accuracy for the macroscopic description of the spatio-temporal behaviour.

Note that, should the volume of the crystal stored in a grid cell (M_{grain}/ρ_p) become larger than the volume of the computational cell (i.e. $\phi^{m+1}>1$), the exceeding mass ($\phi^{m+1}-1$) has to be placed in one of the surrounding computational cells according to the protein concentration distribution (say in the surrounding cell characterized by the lower value of the protein concentration).

3.5 Moving crystals - The OCSVOF method

If the problem under investigation deals with the motion of different phases (absence of gel), there are two fundamentally different approaches that can be used in principle: Eulerian methods use a frame of reference (discretization grid or mesh, control volumes, etc.) fixed in

space, and matter moving through this frame of reference. Lagrangian methods instead use a frame of reference (marker particles) fixed to and moving with the matter.

Eulerian description however is not suitable for problems dealing with the investigation of the evolution of the solid mass displacement of multiple crystals due to gravitational forces. Eulerian methods in fact inevitably suffer from numerical diffusion, which would soon smooth ϕ excessively.

Hybrid techniques however can be used. The first method capable of modelling multi-phase flow, separated by a moving interface (the Marker and Cell (MAC) of Harlow and Welch [9]) was in fact a combination of an Eulerian solution of the basic flow field, with Lagrangian marker particles attached to one phase to distinguish it from the other phase. Instead of MAC, however, Eulerian Volume of Fluid methods (VOF) and Level-Set methods have became popular in the last years (Hirt and Nichols [10], Osher and Sethian [11]). In particular, they have been used for the simulation of typical problems associated to gas/liquid or liquid/liquid systems (e.g. motion of gas-bubble in liquid matrices: Ory et al. [12], etc.) where the interfacial surface tension plays a 'critical role'.

Contrary to the case of classical VOF method, for the present case the time-evolution of the phase variable ϕ is computed according to a Lagrangian description (particle tracking) even if this approach is very expensive. The phase variable ϕ is "transported" according to a Lagrangian equation solved for each of the solid seeds (marker particles) and its value is adjourned according to the algebraic equations of Henisch [7] modelling the release or absorption of protein. The concentration and velocity fields are updated according to an Eulerian description.

Some features of another class of methods (the enthalpy methods) moreover are used here; the enthalpy numerical methods have been developed and made available for the scientific community in the case of growth of inorganic substances, in particular for the case of crystals

grown by thermal solidification of melts under pure diffusive regime or under buoyancy effects (Voller and Prakash [13], Bennonn and Incropera [14], Brent et al. [15]). Here in particular the technique provided by these methods to 'switch off' convective velocities in zones turning to solid phase is used for the bottom of the reactor where the organic crystals tend to be clustered and accumulated.

For this reason the present strategy can be seen as a very hybrid technique and considered an earliest example of a new class of VOF methods specifically developed for the case of growth from supersaturated solutions due to solubility modulation and sedimentation (OCSVOF Organic Crystal Sedimentation Volume of Fraction Method). In the present paper the case of organic growth modeled by algebraic equations is investigated ("macroscopic" description of complex "periodic" phenomena (rhythmic dynamics)). The case of the detailed description of the "local" evolution (evaluation of the surface growth rate distribution for each seed and shape morphology analysis) will be presented in a forthcoming paper [16]. In that case organic growth is governed by a set of differential equations (strictly associated to the surface incorporation kinetics) leading to the introduction of a different type of VOF method with respect to the one introduced here.

In the classical VOF methods, ϕ is 'advected' solving an appropriate Eulerian continuity transport equation, in the enthalpy methods ϕ is computed as function of the temperature obtained solving an appropriate energy equation taking into account the release or absorption of latent heat, for the present method, ϕ is computed according to algebraic equations dealing with mass release or absorption due to solubility modulation and 'transported" according to a Lagrangian description (marker particles). Regarding this aspect note that interpolations (first order polynomial functions not described for the sake of brevity) are required to "link" the "Lagrangian" position of the solid particle with the fixed (Eulerian) points of the computational mesh where the protein concentration is computed.

3.6 Sedimentation:

This paragraph deals with the modelling of the sedimentation process under the assumption that solutal buoyancy convection cannot establish in the protein chamber. The model for the combined sedimentation-convection will be discussed in the next paragraph.

Crystal sedimentation will occur due to a difference between the gravitational force and the viscous resistance. The viscous resistance acting on a solid particle (the crystals are assumed to be spheres) moving with a velocity V_{grain} can be given in dimensional form (the overbar is used to highlight dimensional quantities) by Stokes law as $F_D = 6\pi \overline{R}\ \mu\ \overline{V}_{grain}$ where μ is the coefficient of dynamic viscosity of the solution, $\overline{V}_{grain}$ the velocity of the solid particle of radius R and non-slip conditions are assumed at the particle surface. The gravitational force is given by $F_g = \frac{4}{3}\pi\ \overline{R}^3(\rho_C - \rho_L)g$ where ρ_C and ρ_L are the densities of the crystal and solution, respectively. The equation of motion of sedimenting crystals reads:

$$\frac{4}{3}\pi\ \rho_C \frac{d\left(\overline{R}(\bar{t})^3 \overline{V}_{grain}\right)}{d\bar{t}} = \frac{4}{3}\pi\ \overline{R}^3(\rho_C - \rho_L)g - 6\pi\overline{R(t)}\ \mu\ \overline{V}_{grain} \qquad (9)$$

where $\rho_L = \rho_{H_2 0}(1 + \beta_{lys}\overline{C}_{lys} + \beta_{NaCl}\overline{C}_{NaCl})$ (β_{lys} and β_{NaCl} are the solutal expansion coefficients related to lysozyme and salt respectively); eq. (9) in non-dimensional form reads (the reference velocity is $V_D = D_{lys}/L$):

$$\frac{dV_{grain}}{dt} = \frac{gL^3}{D_{lys}^2}(1 - \frac{\rho_L}{\rho_C}) - \frac{9}{2}Sc\frac{\rho_L}{\rho_C}\frac{V_{grain}}{R(t)^2} - 3\frac{V_{grain}}{R(t)}\frac{dR}{dt} \qquad (10)$$

where $Sc = \nu / D_{lys}$, $R(t) = \frac{1}{L}\sqrt[3]{\frac{3}{4\pi}\frac{M_{grain}(t)}{\rho_p}} = \sqrt[3]{\frac{3}{4\pi}\phi(t)dv}$

In eqs. (9)-(10) the dependence of the radius of the solid particle on the time has been highlighted in order to point out that the size of a sedimenting particle may change during

sedimentation due to further absorption (or release) of mass (M_{grain} is a function of time) as explained in the previous paragraphs.

Eq. (10) has been solved for each crystal (particle tracking) assuming $V_{grain}=0$ and $y=y_{nucl}$ as initial conditions, where y_{nucl} is the position at which nucleation occurs.

Protein crystals are denser than the feeding solution thus on Earth they settle in the computational cells on the bottom of the growth chamber.

If the volume of the mass sedimented in a computational cell is greater than the volume of the cell (i.e. $\phi > 1$), the exceeding mass ($\phi - 1$) has to be placed in one of the surrounding grid cells according to the mass distribution (still in the surrounding cell characterized by the lower value of mass).

3.7 Sedimentation-Convection:

The sedimentation model discussed in the previous paragraph is now improved and further refined by taking into account the effect of convection arising in the protein chamber due to buoyancy forces. The flow is governed by the continuity, Navier-Stokes and species equations, that in non-dimensional conservative form read :

$$\underline{\nabla} \cdot \underline{V} = 0 \tag{11}$$

$$\frac{\partial \underline{V}}{\partial t} = -\underline{\nabla} p - \underline{\nabla} \cdot [\underline{V}\underline{V}] + Sc \ \nabla^2 \underline{V} + Sc \ Ra_{lys} \ C_{lys} + D_{NaCl} / D_{lys} \ Sc \ Ra_{NaCl} \ C_{NaCl} - \frac{1}{\chi} Sc \underline{V} \tag{12}$$

where $Ra_{lys} = \dfrac{g\beta_{lys} L^3 C_{lys(o)}}{\nu D_{lys}}$ and $Ra_{NaCl} = \dfrac{g\beta_{NaCl} L^3 C_{NaCl(o)}}{\nu D_{NaCl}}$

$$\frac{\partial C_{lys}}{\partial t} = -\underline{\nabla} \cdot [\underline{V} C_{lys}] + \nabla^2 C_{lys} \tag{13}$$

$$\frac{\partial C_{NaCl}}{\partial t} = -\underline{\nabla} \cdot [\underline{V} C_{NaCl}] + D_{NaCl} / D_{lys} \ \nabla^2 C_{NaCl} \tag{14}$$

where V and p are the non-dimensional velocity and pressure. The reference pressure is $\rho_{H_2 0} D_{lys}^2/L^2$. Non-slip conditions are imposed on the solid walls.

Eqs. (11-14) subjected to the initial and boundary conditions were solved numerically in primitive variables by a finite-difference method. The domain was discretized with a uniform mesh and the flow field variables defined over a staggered grid. Forward differences in time and central-differencing schemes in space (second order accurate) were used to discretize the partial differential equations, obtaining (superscript n indicates time step):

$$\underline{V}^{n+1} = \underline{V}^{n} + \Delta t\left[-\underline{\nabla}\cdot(\underline{V}\underline{V}) + Sc\nabla^2\underline{V} + Sc\ \ Ra_{lys}\ \ C_{lys} + D_{NaCl}/D_{lys}\ \ Sc\ \ Ra_{NaCl}\ \ C_{NaCl}\right]^n - \Delta t\underline{\nabla}p^n - Sc\frac{1}{\chi}(\underline{V})^{n+1}$$

$$C_{lys}^{\ n+1} = C_{lys}^{\ n} + \Delta t\left[-\underline{\nabla}\cdot\left[\underline{V}C_{lys}\right] + \nabla^2 C_{lys}\right]^n \tag{16}$$

$$C_{NaCl}^{\ n+1} = C_{NaCl}^{\ n} + \Delta t\left[-\underline{\nabla}\cdot\left[\underline{V}C_{NaCl}\right] + D_{NaCl}/D_{lys}\ \nabla^2 C_{NaCl}\right]^n \tag{17}$$

For further details on the numerical method see Ref.[17,18]. The protein and salt distributions at time (n+1) are obtained from Eqs. (16) and (17) after the velocity calculation. The nucleation and precipitation phenomena are taken into account according to the technique described in paragraphs 3.2-3.4. The equation of motion of sedimenting crystals has to be modified in order to take into account the velocity field due to the buoyancy forces

$$\frac{dV_{grain}}{dt} = \frac{gL^3}{D_{lys}^2}(1-\frac{\rho_L}{\rho_C}) - \frac{9}{2}Sc\frac{\rho_L}{\rho_C}\frac{V_{grain}-V}{R(t)^2} - 3\frac{V_{grain}}{R(t)}\frac{dR}{dt} \tag{18}$$

which in discrete form reads:

$$V_{grain}^{n+1} = V_{grain}^{n} + \Delta t\frac{gL^3}{D_{lys}^2}(1-\frac{\rho_L}{\rho_C}) - \Delta t\frac{9}{2}Sc\frac{\rho_L}{\rho_C}\frac{V_{grain}^{n+1}-V^{n+1}}{(R^{n+1})^2} - 3\frac{V_{grain}^{n+1}}{R^{n+1}}\left(R^{n+1}-R^n\right) \tag{19}$$

i.e. it is assumed that, due to the small size of the sedimenting crystals, the velocity field $\underline{V}$ is not affected directly by the motion of these particles and that, viceversa, the sedimenting particles may be accelerated or decelerated by the effect of $\underline{V}$.

The necessary coupling between the convective field $\underline{V}$ and the presence of solid mass is given through the Darcy term added in the momentum equation. Regarding this aspect note that since crystals tend to be clustered and accumulated on the bottom of the reactor a 'permeable' crystalline matrix which coexists with the liquid phase is created there.

An important problem with fixed-grid solution procedures, is accommodating the zero velocity condition in zones occupied by motionless solid mass. Various methods can be used in principle to 'switch off' velocities in computational cells that are becoming solid (or 'switch on' velocities in the reverse case). The approach used here (porosity approach) requires that computational cells filled with solid phase are modeled as a pseudo-porous media, with the porosity χ being a function of ϕ ranging between 0 (fully liquid cell) and 1 (fully solid cell). The term $-Sc\underline{V}/\chi$ in eqs (12) and (15) is the Darcy term added to the momentum equation to eliminate convection in the solid phase. In the present analysis permeability is assumed to vary according to the Carman-Kozeny equation (Bennon and Incropera [14] and Brent et al. [15]).

$$\chi = \frac{(1-\phi)^3}{\phi^2} \tag{20}$$

In the pure solid (ϕ=1) and pure liquid (ϕ=0), equation (20) reduces to the appropriate limits, namely χ=0 and $\chi = \infty$ respectively. In practice the effect of χ is as follows: in full liquid elements $1/\chi$ is zero and has no influence; in elements that are changing phase, the value of χ will dominate over the transient, convective and diffusive components of the momentum equation, thereby forcing them to imitate Carman-Kozeny law; in totally solid elements, the final large value of $1/\chi$ will swamp out all terms in the governing equations and force any velocity predictions effectively to zero. Since the momentum equation is valid throughout the entire domain, explicit consideration need not be given to the solid mass accumulated on the bottom of the crystallization chamber.

Note that, in principle, the OCSVOF method provides reliable results only if the decrease of solution volume due to the crystallization process is negligible (otherwise a source term has to be added to eq. (11)). In the case of inorganic crystal growth, since solvent inclusions in the solid mass are very small, this would occur if the decrease of solution volume was only a few per cent of its initial volume (i.e. if the crystal undergoes only small dimensional changes with respect to the overall dimensions of the cell containing the feeding solution). Fortunately this problem is not remarkable for the case of organic macromolecular substances. Protein crystals, in fact, have widely open structures and incorporate up to 90% by volume of solvent within the network of protein molecules. Macromolecular crystals are mainly composed of solvent. The protein occupies the remaining volume so that the entire crystal is in many ways an ordered gel with extensive interstitial spaces through which solvent may freely diffuse (see e.g. McPherson [1], Rosenberger [2]).

3.8 Program organization

The code has been written entirely in FORTRAN 90, making full use of the advanced concepts provided by the language, such as dynamic data structures and pointers. Thus a much more compact, well-structured, and maintainable code has been obtained.

The numerical solution proceeds in 5 major stages:

1. Solution of the Navier Stokes equations ($\underline{V}^{n+1}$ as function of $\underline{V}^{n}$, C_{lys}^{n} and C_{NaCl}^{n})
2. Solution of the species equations (16) and (17) for protein and salt respectively (C_{lys}^{n+1} and C_{NaCl}^{n+1} are computed as function of the corresponding distributions and of the velocity field at time n).

3. Calculation of the Solubility distribution S^{n+1} (as function of the salt distribution C_{NaCl}^{n+1}) and of the supersaturation $\sigma^{n+1}=C_{lys}^{n+1} / S^{n+1}$.

4. Numerical simulation of the nucleation and further growth or resolution phenomena according to the supersaturation distribution (algebraic model) and consequent adjournment of the local values of protein concentration, phase field ϕ and radius R at time n+1 (see eqs. (6) and (8)). In case new seeds are formed, the size of the arrays storing the information (position, velocity and ϕ) related to moving solid particles is increased in order to take into account the new particles.

5. Solution of eq. (19) for each solid particle; then V_{grain}^{n+1} is used to compute the new position at time n+1: $y^{n+1} = y^n + \Delta t \left(\frac{V_{grain}^{n+1} + V_{grain}^{n}}{2} \right)$.

Note that in the case of gellified phenomena the phase variable ϕ can be handled as an Eulerian variable (it is computed in the same points of the computational grid where the other quantities are evaluated) whereas in the case of sedimentation, ϕ behaves as a Lagrangian variable associated to marker particles and special arrays used to store its position and velocity.

3.9 Validation and grid refinement study

The numerical technique discussed from paragraphs 3.1 to 3.4 has been validated through comparison with the numerical results of [7]. The numerical method described in paragraph 3.7 requires the application of subroutines which have been already used by the authors in previous works and have been widely validated (see e.g. Ref. [17-18]). Finally, further validation has been provided by comparison with experimental observations [19,20].

In this sub-section, moreover, in order to show the numerical convergence of the present algorithm a grid refinement study is presented. The parameter used to measure the sensitivity of the algorithm to the density of the mesh is the number N of crystals in the gellified configuration since it is expected that this number may strongly depend on the resolution of the computational grid.

For the data shown in table 1 and after $2 \cdot 10^5$ s, the algorithm provides the following results: grid 35x70, 115 crystals, grid 40x80, 123 crystals, grid 45x90, 128 crystals, grid 50x105, 128 crystals. The results show that grid convergence is obtained for a grid of 45x90 points.

4. RESULTS AND DISCUSSION

4.1 Crystal distribution

In the gel environment (Fig. 1a) lysozyme precipitation produces crystals distributed along both the horizontal and vertical directions (the time evolution of the phenomenon is shown in Figs.2-4). Fig. 2a shows that after $2 \cdot 10^4$ s, some crystals appear at the interface separating the protein from the salt solution. Correspondingly a “depletion zone” is visible around each solid particle (Fig.3a). These zones, which have low concentration of protein, are produced by lysozyme depletion to create the solid deposits.

The fact that salt diffuses in the protein chamber through the gel interface so that solubility modulation first occur there, explains the presence of solid particles near to the interface rather than in other regions. Due to the distribution of salt at the initial time, solid particles have the largest size in the central part of the interface at the beginning (Fig.2a). In fact for t=0 the salt distribution follows the shape of the gel meniscus whose interface is not horizontal due to surface tension effects, as experimentally observed by [19]. The interface has a minimum protruding in the protein chamber at x=L/2 where the solubility modulation first occurs.

Other solid particles are present on both sides. Their size decreases as the distance from the position x=L/2 increases. Moreover, when the distance from the position x=L/2 increases, the distance between two solid particles becomes lower.

Due to the nucleation phenomenon described above, a “band”, i.e. a region of low protein concentration, having a certain width is created all around the crystals. This band protrudes from the interface in the protein chamber (Fig. 3a) and has a width somehow proportional to the amount of solid mass, since the depletion of the protein concentration distribution is strictly related to the deposits created.

The simulations show that no further nucleation occurs for t in the range from $4 \cdot 10^4$ to $10 \cdot 10^4$ s. Solid deposits however continue to grow thus increasing the extension of the “depleted band”. The absence of further nucleation in the depleted band is due to the local depletion of protein solution. The formation of the first nuclei depletes locally the protein solution; protein diffuses towards nuclei promoting their growth and enlarging the depletion zone. Therefore C_{lys} is decreased and, even if salt diffuses downwards, lowering solubility, further nucleation is prevented as far as $\sigma<\eta$.

Figs. 2b,3b and 4b show that after $12 \cdot 10^4$ seconds new nucleation occurs and a new distribution of solid particles is created. Hereafter solid particles distributions due to nucleation will be referred as “layers” of crystals. Figs. 2b and 3b show that a new layer is created at the lower boundary (where protein concentration is close to the initial value) of the depleted zone related to previous nucleation and further growth of the crystals. This new nucleation occurs when the local concentration of salt is enough to let the local “supersaturation limit” to be overcome by the local protein concentration. Due to nucleation a new “depleted band” appears.

The diffusion of salt through the protein solution leads to further nucleation and growth events. Figs 2c-f, 3c-f and 4c-f show that the phenomenon under investigation is characterized

by a certain degree of periodicity in time and in space. New solid particles are created at the lower boundary of depleted bands when the local concentration of salt has reached a value to let the local protein concentration overcome the "supersaturation limit". It should be pointed out however that the average y distance between two "layers" of crystals is not constant. This one of the reasons for which the term "periodic" should be interpreted with caution and tolerance for the problem under investigation. Strictly speaking, this term demands a period (i.e. a constant time or space interval), something that the phenomena here under discussion fail to show. These phenomena are nevertheless "periodic". The periods are not constant, but they are not random either. The space distance between two consecutive layers, in fact, does not change in random way, but decreases towards the bottom of the protein chamber.

The amplitude is maximum for the first "depleted band", then it is almost constant for the two intermediate bands and then it reaches a minimum for the last band.

Moreover for a fixed layer a certain degree of space periodicity can be highlighted for the x-distribution of the solid particles along the layer. The average distance between two consecutive particles along x is not random. It is the same for the layers 2,3 and 4 whereas the layer 5 is characterized by a very small average x distance with respect to previous layers.

According to the results discussed above, the "density of particles" defined as ratio of the number of particles in a fixed reference volume and the reference volume, is minimum near the interface, constant in the bulk, and maximum near the bottom of the protein chamber.

4.2 Effect of the value of η

The results discussed above have been obtained under the constraint that the ratio η between the supersaturation limit and the solubility is fixed (η=3). This assumption is supported by the good agreement between the numerical results obtained with the present code and others obtained experimentally [19]. However in order to establish the importance of the effect of η,

its value has been changed according to Table 2. The numerical results show that the parameter η can influence the number of locations where nucleation occurs (i.e. the number of crystals produced due to nucleation) and their spatial distribution.

For η =3, the number of crystals is 128. They are organized in five layers corresponding to the existence of four "depleted bands" of different amplitude. The amplitude is maximum for the first band, then it is almost constant for the two intermediate bands and then it reaches a minimum for the last band. For η =2, the number of crystals is 140. Their number is similar (within 10%) as for the previous case, but their spatial organization is completely different. The amplitude of the first depleted band is almost the same of that of the subsequent ones. The distribution of crystals is more uniform. They are organized in eight layers corresponding to the existence of seven "depleted bands", whose amplitude is different. However the space distance between two consecutive layers decreases continuously towards the bottom of the protein chamber without step changes. Moreover, the average x distance among particles placed on the same layer is of the same order of the y distance among consecutive layers. For this reason the "density of particles" increases continuously from the surface to the bottom of the protein chamber where it reaches its maximum (see Fig.5a). If η is further decreased, the number of crystals increases (see Table 2) and the amplitude of the depleted bands tends to become constant. For η =1.1, the density of particles is almost uniform in the entire protein chamber (Fig. 5b). If η is increased the behaviour is the opposite. For η=4, the number of crystals is reduced to 96. They are organized in five layers. This distribution is similar to that observed in the case η=3, but now the ratio between the amplitudes of the first and of the second depleted band is very large if compared with the case η=3 (Fig.5c). For η=5 (Fig.5d), only one layer of six crystals is produced near the surface of the gel within the fixed observation time ($t=2\cdot10^5$ s).

It seems that the effect of η is to make the crystal distribution more uniform if it is decreased and, on the contrary, to allow step changes if it is increased. This behaviour can be explained according to the dynamics of the nucleation process. New solid particles are created on the lower boundary of depleted bands when the local concentration of salt has lowered the supersaturation limit in order to let it to be overcome by the local protein concentration. According to this behaviour, one may expect that if the parameter η is decreased, the distance between consecutive layers of crystals is reduced (and the distribution of solid particles becomes more uniform) since a lower value of the concentration of salt is required to overcome the supersaturation limit (that has been reduced due to the decrease of η). A lower value of concentration of salt, in fact, implies a lower time interval required to let the salt diffuse up to that value. Viceversa, if the parameter η is increased, a larger value of concentration of salt will be required to obtain nucleation and therefore a larger time interval is required to let the salt diffuse. Therefore the distance between consecutive layers of crystals and in particular the amplitude of the first band are increased. A further paper aimed at tuning the optimum value of η which matches laboratory experimental results is in progress [20].

4.3 Sedimentation

Consider the case where gel matrix is not used in the protein chamber (see Fig. 1b). Buoyancy-driven convection has been neglected for the first group of simulations.

Since protein crystals are denser than feeding solution, sedimentation occurs. In this case the phenomena under investigation do not show the complex Liesegang patterns described in the previous paragraphs, Liesegang patterns being destroyed by the crystal sedimentation. The solid particles settle in the growth chamber. The lower boundary of the protein chamber being the interface of gel used to fill the salt chamber, the crystals sediment on this interface. This is clearly shown in Figs.6 where the thickness of the layer of crystals sedimented on the bottom

is an increasing function of time due to the continuous incoming mass. Fig. 6a show that the first nucleation occurs at the free interface for the same reasons explained in the previous paragraphs. Solid particles condense on the interface and then, if the local value of concentration is larger than the solubility, they grow due to further precipitation of protein. As time passes and salt diffuses in the protein chamber, the "nucleation front" (external boundary of the zone where new particles nucleate) migrates towards the top of the protein chamber and other nucleation occurs far from the interface. Similarly to the configuration investigated in the previous paragraph (i.e. crystals locked on the gel matrix), each nucleation occurring in the protein chamber gives rise to a depletion zone around the location where the solid particle has condensed. For the present case, however the solid particle is not locked on its initial position and for this reason it leaves the position where nucleation has occurred. During its fall to the bottom, the solid particle depletes of protein the surrounding liquid. For this reason a wake is produced beyond the sedimenting particle and a small depletion zone highlights its initial position. This is clearly visible in Figs. 7 for time equal to $13.2 \cdot 10^4$ and $14.4 \cdot 10^4$ seconds.

If sedimentation is possible, the numerical results show that the "rate of depletion" related to the propagation of the nucleation front towards the top of the protein chamber is lower than that for the case described in paragraph 4.1. In fact, further depletion due to the phenomenon of subsequent precipitation is negligible in the present case (it simply applies to the wakes beyond the sedimenting particles). Due to the sedimentation process, once solid particles are created, they leave regions of high protein concentration where further precipitation could occur. Solid particles reach the bottom of the protein chamber where the concentration is low due to previous protein absorption. Since all the particles tend to be clustered and accumulated in a same zone of low protein concentration, the possibility of further precipitation and consequent size augmenting is very reduced with respect to the case of

crystals locked in the matrix. For the reasons discussed above, consequently, the final value of the protein concentration in the bulk of the chamber tends to be higher than the case of locked crystals, as shown in Fig. 7f, which can be compared to Fig. 3f.

4.4 Sedimentation-Convection

Fig. 8 shows the time-evolution of the density profile along y in the protein chamber (at each station y the density, computed as $\rho_L = \rho_{H_2 0}(1 + \beta_{lys}\overline{C}_{lys} + \beta_{NaCl}\overline{C}_{NaCl})$, has been averaged along x). Each profile has been obtained under the assumption of protein chamber free of solutal buoyancy convection. At the beginning (t=4000 [s]) the density has a maximum on the gel interface and then it decreases to a minimum on the top of the protein chamber. This density distribution is related to the diffusion of salt through the gel interface. For t<4000 [s], in fact protein depletion due to nucleation phenomena is negligible and density is increased near the gel interface by salt diffusing in the protein chamber. From a fluid-dynamic point of view this situation is stable. In fact buoyancy forces act to slow down fluid denser than the surrounding.

For t= 24000 [s] the density profile is no longer decreasing from the gel interface towards the top of the protein chamber. It increases, reaches a maximum at 2 [mm] from the gel interface and then it decreases towards the top. This behaviour is the result of two counteracting effects: lysozyme is depleted due to the nucleation process thus reducing the density; salt diffuses in the protein chamber through the gel interface thus increasing the density. The latter effect prevails in zones where the nucleation phenomena have not occurred yet (i.e. between the nucleation front and the top of the protein chamber). For t=4000 [s] the nucleation front is located on the gel interface, for t=24000 [s] it is located at a distance d=0.2 [cm]. This explains why for the first case the maximum of the density occurs on the gel interface whereas for the latter it occurs in the bulk of the protein chamber. Fig. 8 shows that, as time

passes, the maximum of the density migrates towards the top of the protein chamber. This behaviour, according to the discussion above, is due to the migration towards the top of the nucleation front. For t=1.76 10^5 s the maximum reaches the top of the protein chamber and for a further increase of the time the shape of the density profile is increasing from the gel interface to the top of the protein chamber.

These results suggest that, for t>4000, onset of convection is possible due to buoyancy forces associated to the inversion in the density profile. For this reason simulations have been carried out taking into account the solution of the non-linear and time-dependent incompressible Navier-Stokes equations.

The numerical results show that vortex cells arise. The region between the gel interface and the maximum of density corresponds in fact to favourable conditions for the onset of flow instability since some fluid layers are located above others with lower density. Viceversa the region between the maximum and the top of the chamber corresponds to conditions unfavourable to convection. Figs. 9a and 9b show the presence of rolls, which at the beginning do not extend over the entire bulk of the protein chamber but remain confined to a region of favourable conditions for the onset of convection. As time passes, the extension of this region increases due to the migration of the nucleation front and the vortex rolls expand to become pervasive throughout the bulk of the protein chamber as shown in Figs. 9c-f for different times.

Regarding the lysozyme concentration distribution (Figs. 10), the simulations point out that the vortex rolls (velocities are of the order of 10^{-1} [cm/s]) add some weak distortion to the corresponding concentration contour-lines and make the crystals distribution on the bottom of the protein chamber (Figs. 9c-f) non symmetric with respect to the point x=L/2.

5. CONCLUSIONS

This study deepen the understanding of crystal growth of lysozyme that occurs by diffusion of the precipitant agent into the protein solution. In particular, the non-linear dynamics of the transient behaviour of this process is investigated. The crystallization process has been presented and analyzed under two different conditions: crystal sedimentation prevented by the use agarose gel and protein chamber free of gel (sedimentation allowed).

The analysis has required the application of already existing mathematical models and appropriate numerical methods to handle the complex phenomena related to protein nucleation and further precipitation or resolution according to the protein concentration distribution and the supersaturation limit. Further to these models, novel numerical techniques and methods have been introduced in the case of sedimentation to investigate the motion of the crystals due to the combined effect of gravitational force and viscous drag, the interaction of this motion with the concentration field and the interaction between depletion phenomena related to nucleation and the onset of convection. The present strategy can be seen as a very hybrid technique and considered an earliest example of a new class of VOF methods specifically developed for the case of growth from supersaturated solutions due to solubility modulation and sedimentation (OCSVOF Organic Crystal Sedimentation Volume of Fraction Method).

The numerical simulations show that, if sedimentation is prevented by the gel, lysozyme precipitates to produce crystals distributed along both the horizontal and vertical directions. As expected, the phenomenon under investigation is characterized by a certain degree of periodicity in time and in space, analogous to the “Liesegang rings”. The bands of Liesegang patterns however are not spatially uniform. Nucleating particles deplete their surroundings of protein which causes a drop in the local level of supersaturation such that the nucleation rate falls in the neighbourhood, leading naturally to a spacing between regions of nucleation that

gives rise to the alternate presence of depleted bands and layers of crystals. New solid particles are created on the lower boundary of depleted bands when the local concentration of salt has reached a value to let the local protein concentration overcome the "supersaturation limit". The numerical simulations show moreover that the further growth of particles after their nucleation, i.e. the increase of the solid particles size, is governed by the delicate balance between counteracting effects. The influence of these effects has been discussed in detail.

If sedimentation is allowed, solid particles condense on the interface and then, if the local value of concentration is larger than the solubility, they grow due to further precipitation of protein. As time passes and salt diffuses in the protein chamber, nucleation occurs far from the interface. However the solid particle are not locked on their initial position and for this reason they leave the position where nucleation has occurred. During the fall to the bottom, the solid particles deplete of protein the surrounding liquid. For this reason a wake is produced beyond the sedimenting particles. The final value of the protein concentration in the bulk of the chamber tends to be higher with respect to the case of locked crystals. This behaviour has been explained according to the fact that all the solid particles tend to be clustered and accumulated in a same zone of low protein concentration, reducing thus the possibility of further precipitation and consequent size augmenting with respect to the case of locked crystals. If convection due to buoyancy forces is taken into account, the results show that convective cells arise in the protein chamber due to local inversions in the density distribution. The complex dynamics related to the interaction between the onset of convection and the nucleation phenomena have been investigated.

6. ACKNOWLEDGEMENTS

The authors would like to thank the Referees for their constructive comments, Dr. Luigi Carotenuto and Dr. Chiara Piccolo (from MARS) for the useful information provided on

phenomenologies observed experimentally and on the configuration of typical experiments and Professor J.M. Garcìa-Ruiz for his precious suggestions. The present work has been supported by the European Space Agency (ESA) and the Italian Space Agency (ASI).

7. REFERENCES

[1] A. McPherson, 'Current approaches to macromolecular crystallization', Eur. J. Biochem, Vol. 189, pp. 1-23, 1990.

[2] F. Rosenberger, 'Inorganic and protein crystal growth: similarities and differences', J. Cryst. Growth, Vol. 76, pp. 618-636, 1986.

[3] A. Monaco A., F. Rosenberger, 'Growth and etching kinetics of tetragonal lysozyme', J. Cryst. Growth, Vol. 129, pp. 465-484, 1993.

[4] M. L. Pusey, R. S. Snyder, R. Naumann, 'Protein crystal growth: growth kinetics for tetragonal lysozyme crystals', Journal of Biological Chemistry, Vol. 261 (14), pp. 6524-6529, 1986.

[5] H.K. Henisch, J.M. Garcìa-Ruiz, "Crystal growth in gels and Liesegang ring formation: Crystallization criteria and successive precipitation", Journal of Crystal Growth, Vol. 75 , pp. 203-211, 1986.

[6] F. Otàlora, J.M., Garcìa-Ruiz, "Crystal growth studies in microgravity with the APCF: Computer simulation and transport dynamics", Journal of Crystal Growth, Vol. 182, pp. 141-154, 1997.

[7] H. K. Henisch, "Periodic Precipitation: a microcomputer analysis of transport and reaction processes in diffusion media with software development", Pergamon Press, 1991.

[8] O. Galkin, P. G. Vekilov, "Direct determination of the nucleation rates of protein crystals", J. Phys. Chem. B, Vol. 103, pp. 10965-10971, 1999.

[9] F.H. Harlow, J.E. Welch, 'Numerical calculation of time-dependent viscous incompressible flow with free surface", Phys. Fluids, Vol. 8, pp. 2182-2189, 1965.

[10] C.W. Hirt, B.D. Nichols, 'Volume of Fluid (VOF) Method for the Dynamics of Free Boundaries', J. Comput. Phys., Vol. 39, pp. 201-225, 1981.

[11] S. Osher, J.A. Sethian, ‘Fronts propagating with curvature-dependent speed: Algorithms based on Hamilton-Jacobi formulations’, J. Comput. Phys., Vol. 79, pp. 12-49, 1988.

[12] E. Ory, H. Yuan, A. Prosperetti, S. Popinet and S. Zaleski, ‘Growth and collapse of a vapor bubble in a narrow tube’, Phys.Fluids, Vol. 12, pp. 1268-1277, 2000.

[13] V. R. Voller, C. Prakash, ‘A fixed grid numerical modelling methodology for convection-diffusion mushy region phase-change problems’, Int. J. Heat Mass Transfer, Vol. 30 (8), pp. 1709-1719, 1987.

[14] W.D. Bennon, F.P. Incropera, ‘A continuum model for momentum, heat and species transport in binary solid-liquid phase change systems-I. Model formulation’, Int.J.Heat Mass Transfer, Vol. 30 (10), pp. 2161-2170, 1987.

[15] A.D. Brent, V.R. Voller, J. Reid, ‘Enthalpy-porosity technique for modelling convection-diffusion phase change: application to the melting of a pure metal’, Num. Heat Transf., Vol. 13, pp. 297-318, 1988.

[16] M. Lappa, “Fluid Mechanics of Protein Engineering”, J. Fluid Mech. (2002 submitted).

[17] M. Lappa; "Strategies for parallelizing the three-dimensional Navier-Stokes equations on the Cray T3E "; *Science and Supercomputing* at CINECA (1997), M. Voli Editor, Bologna, Vo. 11, pp. 326-340.

[18] M. Lappa, R. Savino and R. Monti; "Three-dimensional numerical simulation of Marangoni instabilities in liquid bridges: influence of geometrical aspect ratio"**;** *Int. J. Num. Meth. Fluids*, vol 36 (1), pp. 53-90, 2001.

[19] C.Piccolo, M. Lappa, A. Tortora, D. Castagnolo, L. Carotenuto, “Non-linear behaviour of lysozyme crystallization”, Physica A, vol. 314, no 1-4, pp. 636-645, 2002.

[20] M. Lappa, C. Piccolo, L. Carotenuto, “Periodic precipitation and sedimentation of lysozyme: numerical and experimental analysis of the non-linear behaviour”, *J. Cryst. Growth* (2002 submitted)

L [cm]	1
H [cm]	2.8
Width [cm]	0.1
Height of the protein chamber h [cm]	1.4
D_{lys} [cm^2/s]	10^{-6}
D_{NaCl} [cm^2/s]	10^{-5}
ν [cm^2/s]	$8.63 \cdot 10^{-3}$
ρ_c [g/cm^3]	1.2
β_{lys} [$(g/cm^3)^{-1}$]	0.3
β_{NaCl} [$(g/cm^3)^{-1}$]	0.6
$C_{lys(o)}$ [g/cm^3]	$4 \cdot 10^{-2}$
$C_{NaCl(o)}$ [g/cm^3]	$7 \cdot 10^{-2}$
Computational points along x	45
Computational points along y	90

Table 1: data used as input for the numerical computations

η	Number of solid particles after $2 \cdot 10^5$ s
1.1	574
2	140
3	128
4	96
5	6

Table 2: Effect of the parameter η

List of captions

Fig.1: sketch of the configurations: (a) no sedimentation allowed (b) Lysozyme sedimenting on the gel interface.

Fig.2: Pattern of crystals (gellified conditions): (a)– Time=$2x10^4$ s, (b)– Time=$12x10^4$ s, (c)– Time=$13.2x10^4$ s, (d)– Time=$14x10^4$ s, (e)– Time=$14.4x10^4$ s, (f)– Time=$19.6x10^4$ s (salt chamber located on the top of the protein chamber).

Fig.3: Non-dimensional protein concentration contour lines (gellified conditions): (a)– Time=$2x10^4$ s, (b)– Time=$12x10^4$ s, (c)– Time=$13.2x10^4$ s, (d)– Time=$14x10^4$ s, (e)– Time=$14.4x10^4$ s, (f)– Time=$19.6x10^4$ s (salt chamber located on the top of the protein chamber).

Fig.4: Supersaturation contour lines (gellified conditions): (a)– Time=$2x10^4$ s, (b)– Time=$12x10^4$ s, (c)– Time=$13.2x10^4$ s, (d)– Time=$14x10^4$ s, (e)– Time=$14.4x10^4$ s, (f)– Time=$19.6x10^4$ s (salt chamber located on the top of the protein chamber).

Fig.5: Pattern of crystals: (a) η=2, t=$2x10^5$ s, (b) η=1.1, t=$2x10^5$ s, (c) η=4, t=$2x10^5$ s, (d) η=5, t=$2x10^5$ s.

Fig.6: Pattern of crystals (sedimentation): (a)– Time=$2x10^4$ s, (b)– Time=$8x10^4$ s, (c)– Time=$12x10^4$ s, (d)– Time=$13.2x10^4$ s, (e)– Time=$14.4x10^4$ s, (f)– Time=$19.2x10^4$ s (salt chamber located on the bottom of the protein chamber).

Fig.7: Non-dimensional protein concentration contour lines (sedimentation): Time=$2x10^4$ s, (b)– Time=$8x10^4$ s, (c)– Time=$12x10^4$ s, (d)– Time=$13.2x10^4$ s, (e)– Time=$14.4x10^4$ s, (f)– Time=$19.2x10^4$ s (salt chamber located on the bottom of the protein chamber).

Fig.8: density profile versus time in the protein chamber.

Fig.9: Pattern of crystals (sedimentation and convection): (a)– Time=$2x10^4$ s, (b)– Time=$8x10^4$ s, (c)– Time=$10.4x10^4$ s, (d)– Time=$11.2x10^4$ s, (e)– Time=$14x10^4$ s, (f)– Time=$18x10^4$ s (salt chamber located on the bottom of the protein chamber).

Fig.10: Non-dimensional protein concentration contour lines (sedimentation and convection): (a)– Time=$2x10^4$ s, (b)– Time=$8x10^4$ s, (c)– Time=$10.4x10^4$ s, (d)– Time=$11.2x10^4$ s, (e)– Time=$14x10^4$ s, (f)– Time=$18x10^4$ s (salt chamber located on the bottom of the protein chamber).

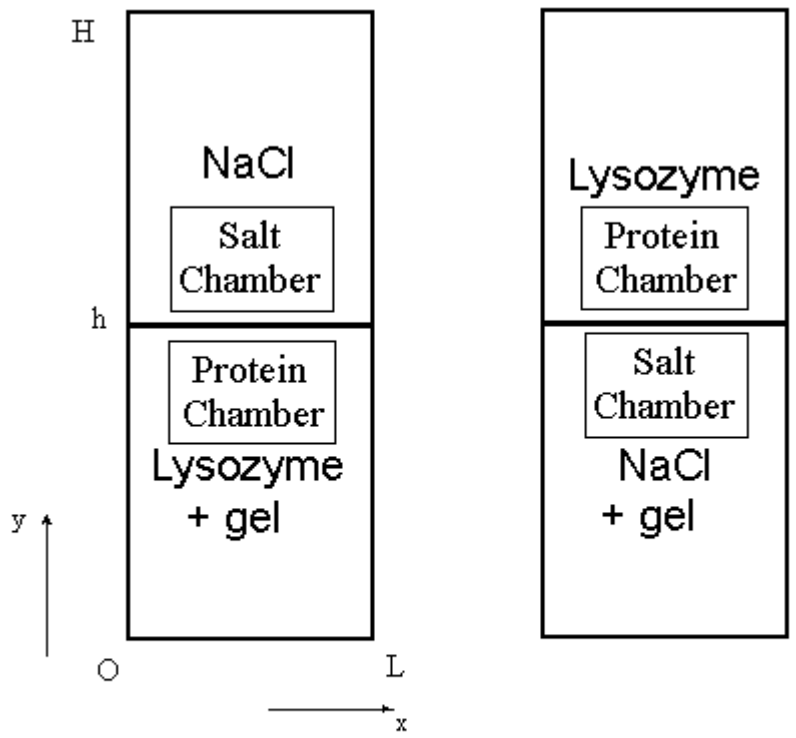

Fig.1: Sketch of the configurations: (a) no sedimentation allowed (b) Lysozyme sedimenting on the gel interface

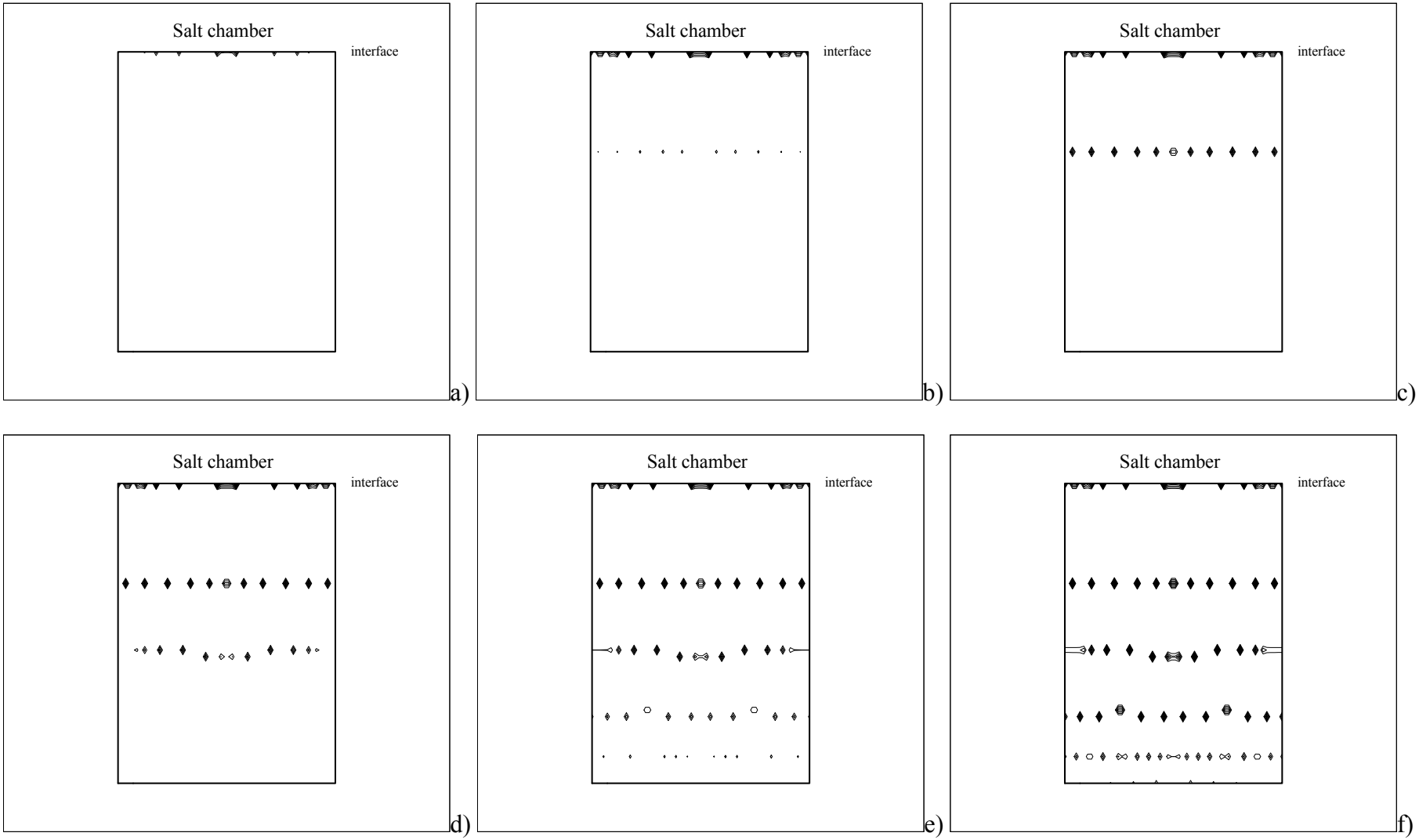

Fig.2: Pattern of crystals (gellified conditions): (a)– Time=$2x10^4$ s, (b)– Time=$12x10^4$ s, (c)– Time=$13.2x10^4$ s, (d)– Time=$14x10^4$ s, (e)– Time=$14.4x10^4$ s, (f)– Time=$19.6x10^4$ s (salt chamber located on the top of the protein chamber).

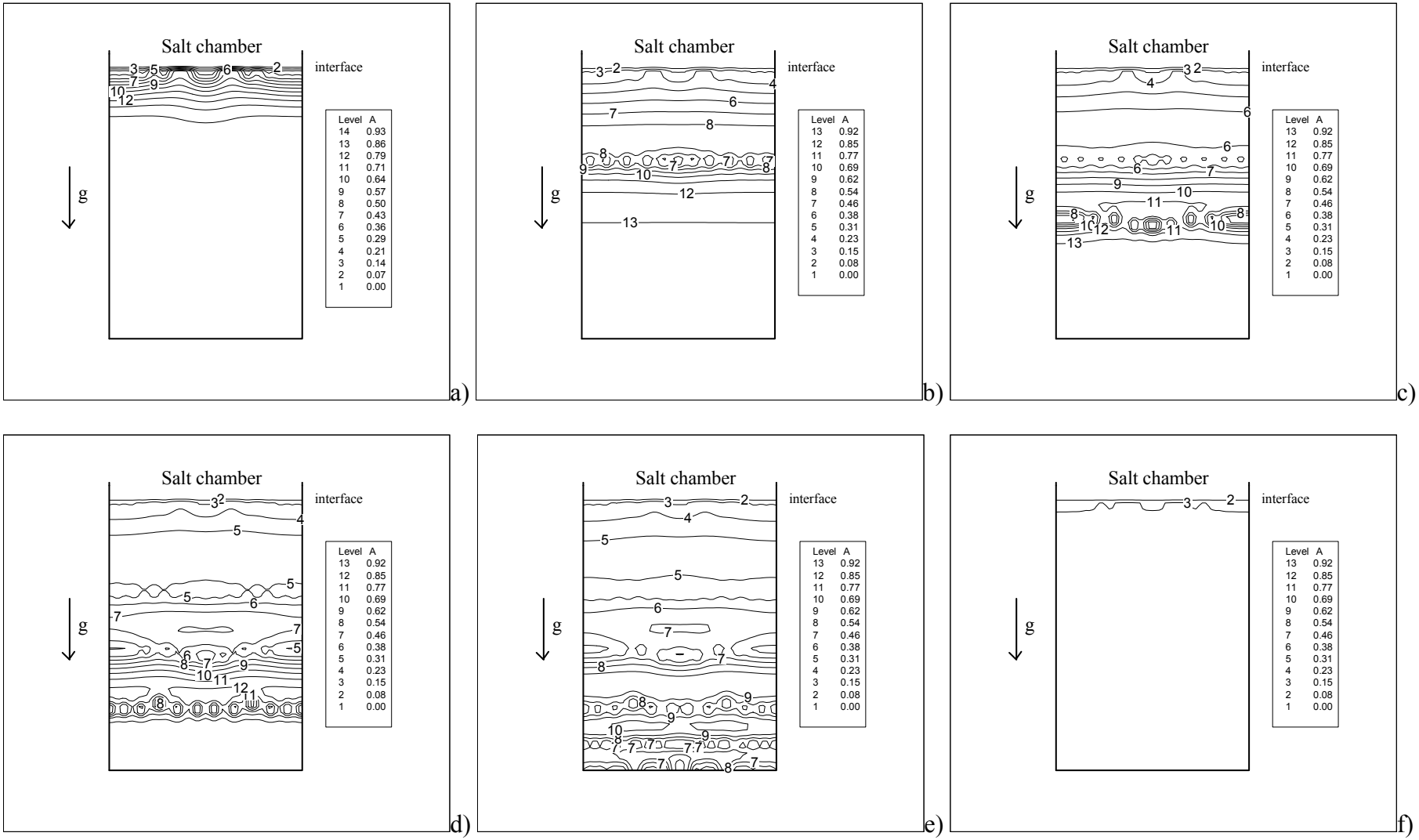

Fig.3: Non-dimensional protein concentration contour lines (gellified conditions): (a)– Time=2x10^4 s, (b)– Time=12x10^4 s, (c)– Time=13.2x10^4 s, (d)– Time=14x10^4 s, (e)– Time=14.4x10^4 s, (f)– Time=19.6x10^4 s (salt chamber located on the top of the protein chamber).

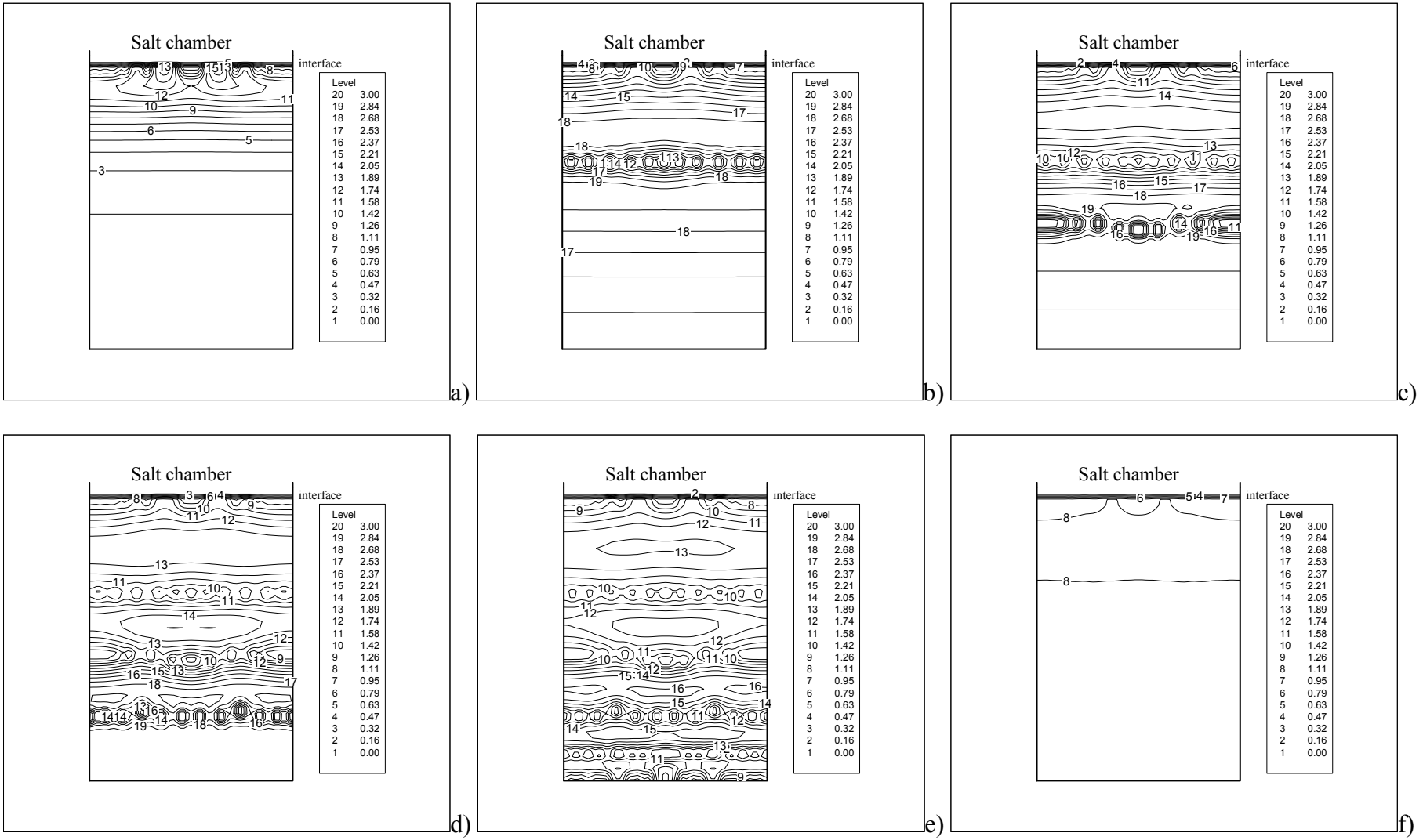

Fig.4: Supersaturation contour lines (gellified conditions): (a)– Time=2x10^4 s, (b)– Time=12x10^4 s, (c)– Time=13.2x10^4 s, (d)– Time=14x10^4 s, (e)– Time=14.4x10^4 s, (f)– Time=19.6x10^4 s (salt chamber located on the top of the protein chamber).

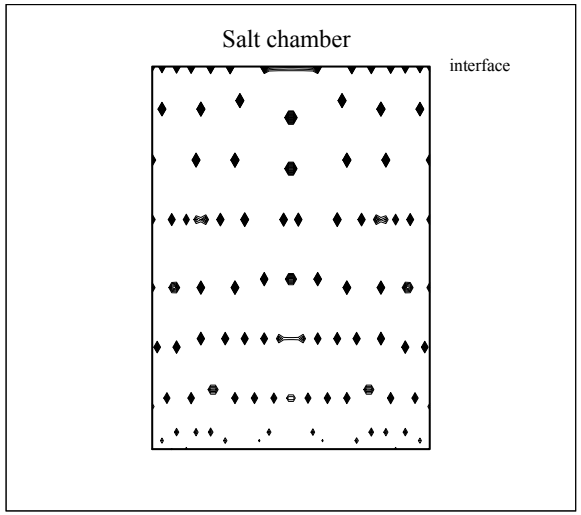

Fig.5a: Pattern of crystals (η=2, t=2x10^5 s)

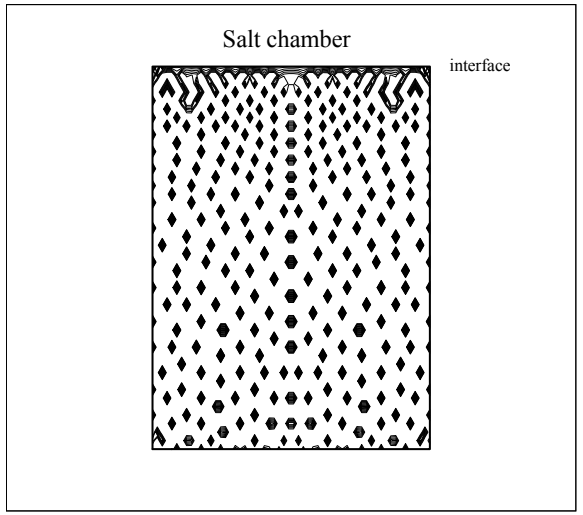

Fig.5b: Pattern of crystals (η=1.1, t=2x10^5 s)

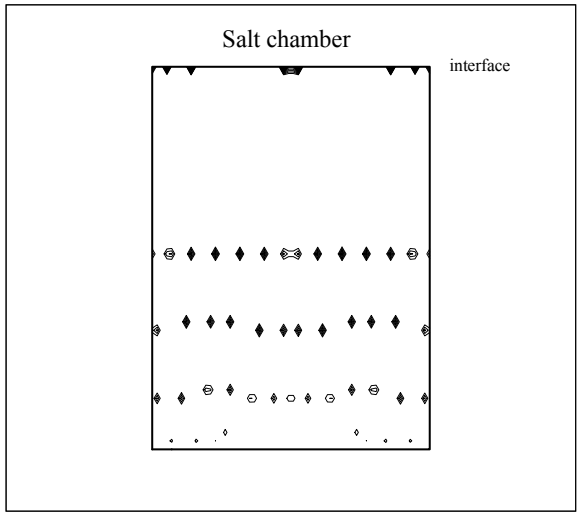

Fig.5c: Pattern of crystals (η=4, t=2x10^5 s)

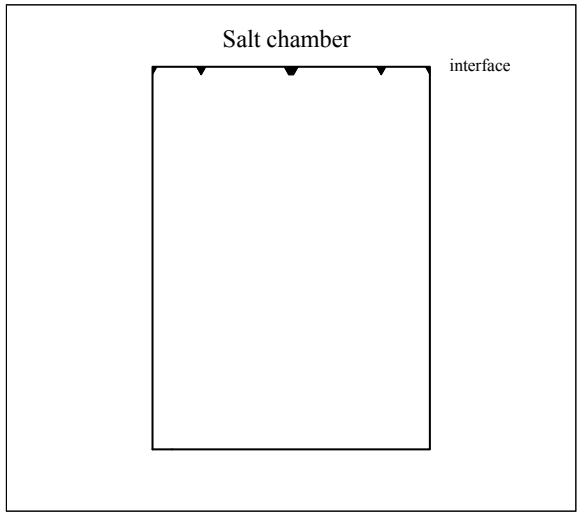

Fig.5d: Pattern of crystals (η=5, t=2x10^5 s)

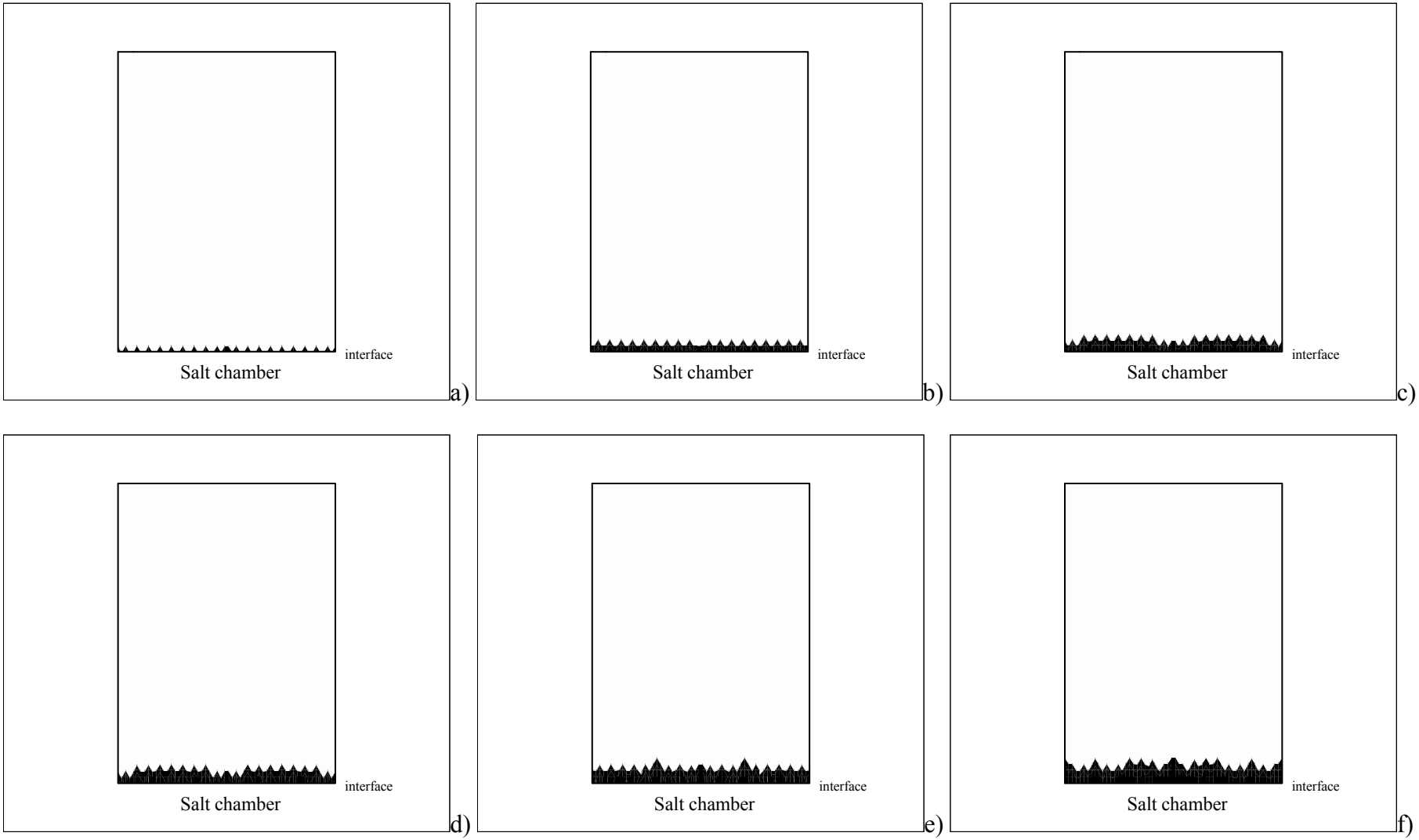

Fig.6: Pattern of crystals (sedimentation): (a)– Time=$2x10^4$ s, (b)– Time=$8x10^4$ s, (c)– Time=$12x10^4$ s, (d)– Time=$13.2x10^4$ s, (e)– Time=$14.4x10^4$ s, (f)– Time=$19.2x10^4$ s (salt chamber located on the bottom of the protein chamber).

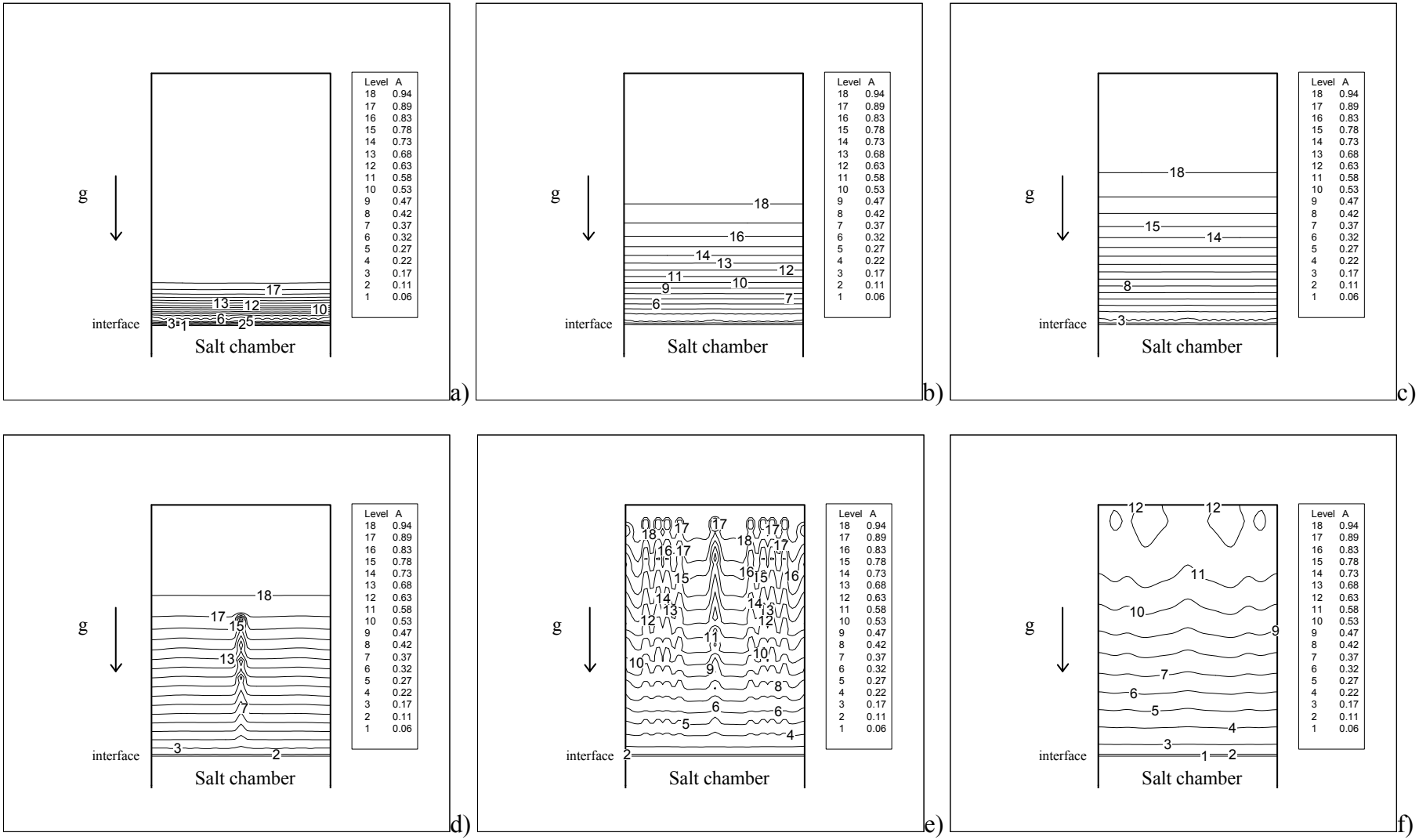

Fig.7: Non-dimensional protein concentration contour lines (sedimentation): Time=2x10^4 s, (b)– Time=8x10^4 s, (c)– Time=12x10^4 s, (d)– Time=13.2x10^4 s, (e)– Time=14.4x10^4 s, (f)– Time=19.2x10^4 s (salt chamber located on the bottom of the protein chamber).

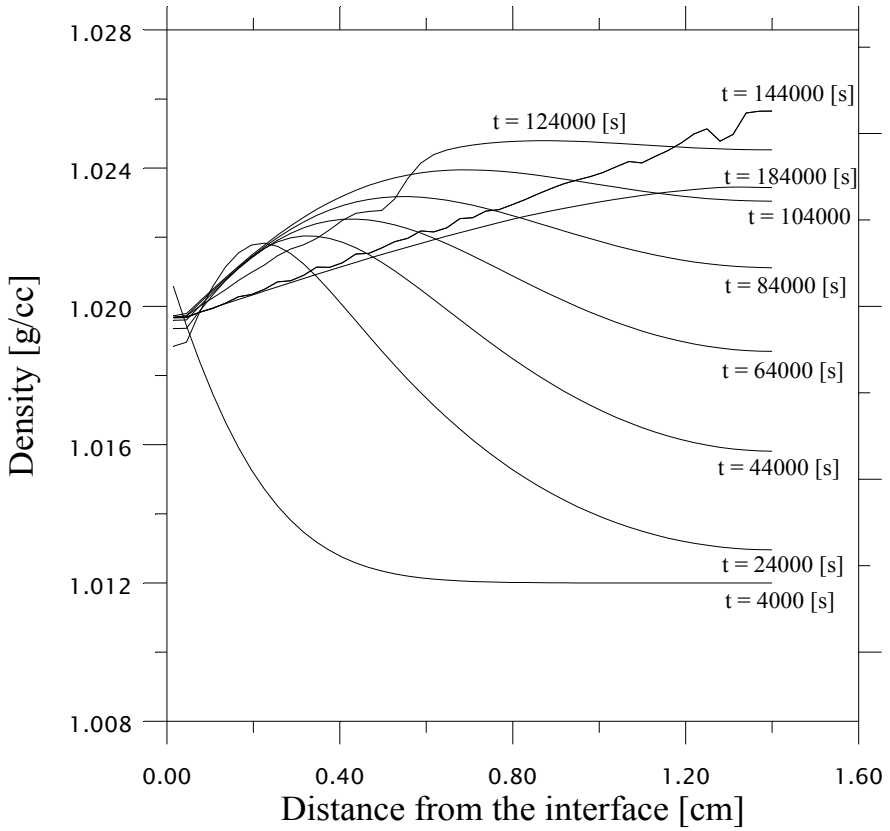

Fig.8: Density profile versus time in the protein chamber

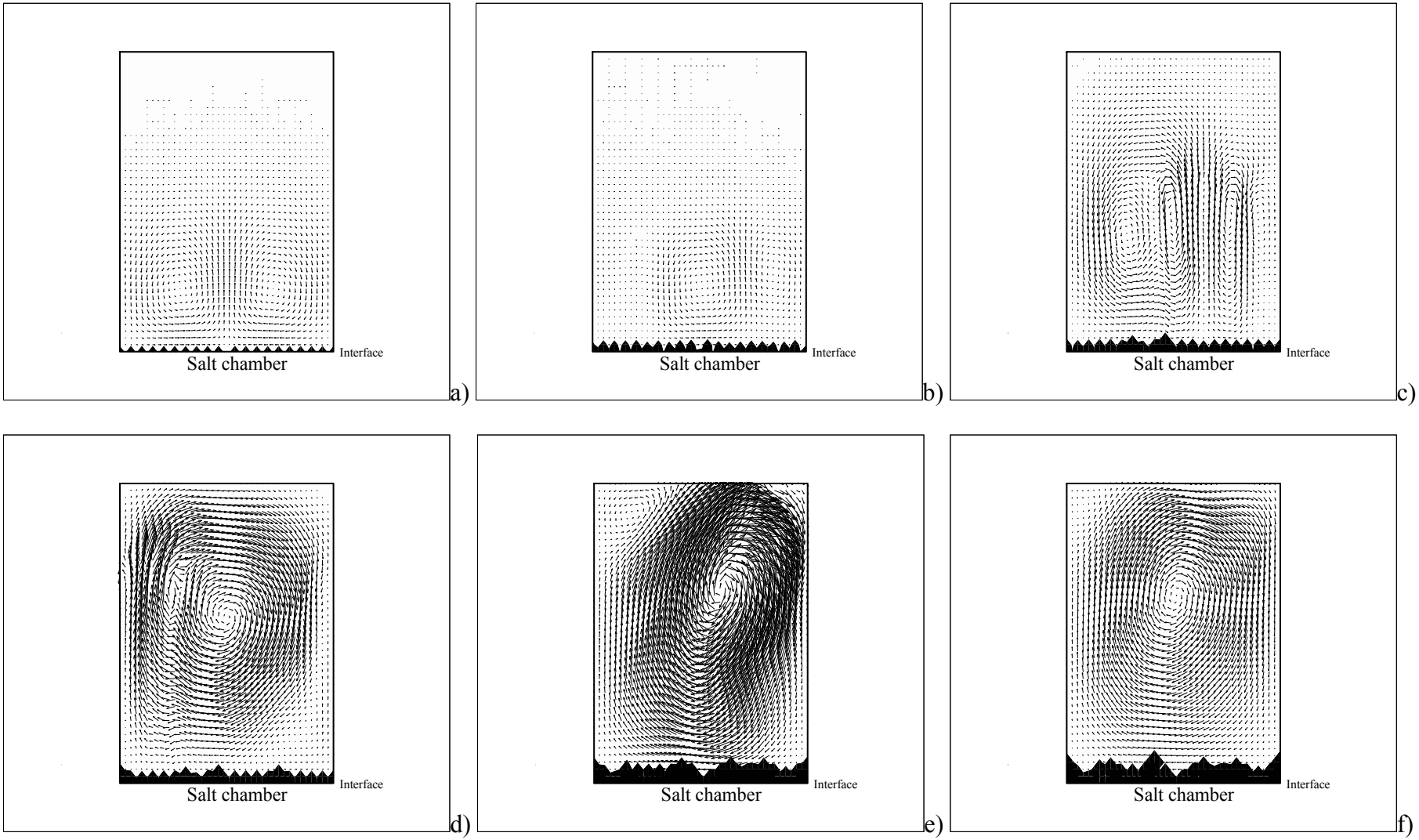

Fig.9: Crystals distribution (sedimentation and convection): (a)– Time=$2x10^4$ s, (b)– Time=$8x10^4$ s, (c)– Time=$10.4x10^4$ s, (d)– Time=$11.2x10^4$ s, (e)– Time=$14x10^4$ s, (f)– Time=$18x10^4$ s (salt chamber located on the bottom of the protein chamber).

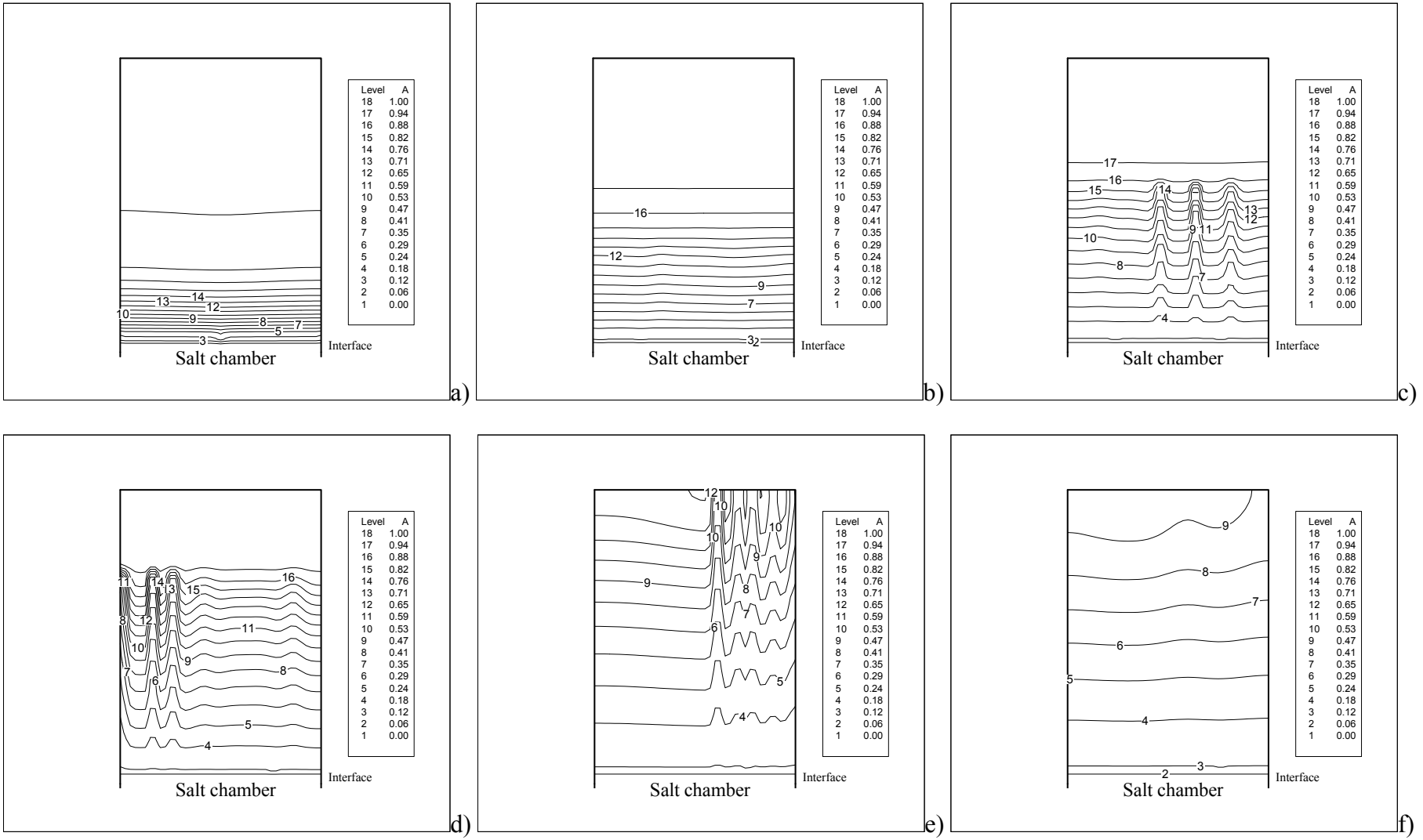

Fig.10: Non-dimensional protein concentration contour lines (sedimentation and convection): (a)– Time=$2x10^4$ s, (b)– Time=$8x10^4$ s, (c)– Time=$10.4x10^4$ s, (d)– Time=$11.2x10^4$ s, (e)– Time=$14x10^4$ s, (f)– Time=$18x10^4$ s (salt chamber located on the bottom of the protein chamber).